



Title	A regional climatology of the aerosols for MERIS atmospheric correction: Inherent Optical Properties (IOP)
Version	0.1
Author(s) and affiliation(s)	F. Zagolski, O. Aznay and R. Santer ADRINORD
Distribution	Public report

Executive summary

The AERONET stations in the 2 Seas region were analyzed to describe the aerosol optical properties. Two approaches were used: one provided by ADRINORD which inverts the measurements to provide the relevant IOPs and another available on the AERONET web server. The two sets are analyzed in order to provide a representative set of aerosol models, set to be used as auxiliary data in the atmospheric correction of satellite colour images.

Acronyms

AERONET	AERosol RObotic NETwork
ALM	Almucantar
AOT	Aerosol Optical Thickness
APF	Aerosol Phase Function
BOA	Bottom Of Atmosphere
IOP	Inherent Optical Properties
IOPA	Inherent Optical Properties of Aerosols
LUT	Look Up Table
MERIS	MEdium Resolution Imaging Spectrometer
NIR	Near-Infrared
PPL	Principal PLane
RMS	Root Mean Square error
SAM	Standard Aerosol Model
TOA	Top Of Atmosphere

Symbols

α	Angström Coefficient
Θ	Scattering angle
τ	Optical thickness
ϖ_0	Single scattering albedo
$P(\Theta)$	Phase function
λ	Wavelength
m	Real part of the refractive index
ε	Gordon Coefficient

Figures and tables

Table 1: Number of sequences per station as described above for AEROPA

Table 2: For each of the 16 class, we give the nominal centre in α , the number N of sequences per class, the Angstroem coefficients first between 670 nm and 870 nm; second between 440 nm and 670 nm.

Table 3: AOT (mean and sigma) in AAOT at 3 wavelengths and $\alpha(670,870)$

Table 4: P_a (mean and sigma) in AAOT at 3 wavelengths and 3 scattering angles

Table 5: $\varepsilon(440,870)$ (mean and sigma) in AAOT at 3 scattering angles

Table 6: Number of WOPAER sequences at each of the 16 classes (plus the total) for AAOT (left block) and the 2Seas region (right block) with N_0 : number of sequences before filtering; N_1 , N_2 , N_3 number of sequences after filtering respectively at 412 nm, 670 nm and 870 nm

Figure 1: single scattering albedo versus the Angstroem coefficient for the Venice AERONET site.

Figure 2: Aerosol phase function in two spectral bands for the 3562 sequences

Figure 3: Aerosol phase function in two spectral bands for the 837 sequences

Figure 4: Aerosol phase function at 870 nm for three scattering angles: 90°; 120° and 150°.

Figure 5: $\varepsilon(440,670)$ versus $\varepsilon(670,870)$ for three scattering angle

Figure 6: $\varepsilon(440,870)$ for three scattering angles with the mean value (blue diamond), the maximum (red square) and minimum (green triangle) values at one sigma

Figure 8: Dispersion of $\varepsilon(440,870)$ in AAOT at three scattering angles Figure 7: Dispersion of P_a in AAOT at two wavelengths for $\Theta=90^\circ$ and at 870 nm for $\Theta=150^\circ$.

Figure 9: Comparison of P_a versus the Angstroem coefficient $\alpha(670,870)$ with the mean value for AAOT (blue diamond) and for the 2seas (green triangle) and the maximum values value for AAOT (red square) and for the 2seas (cross)

Figure 10: Same as figure 9 but on $\varepsilon(440,870)$

Figure 11: Retrieval of the aerosol phase function for the class $\alpha(1.4-1.5)$ at 440 nm (upper plot) and 870 nm in the principal plane (green triangles), the almucantar 1 (blue diamond) and 2 (red square)

Figure 12: Successive filtering of P_a for the class $\alpha(1.4-1.5)$

Figure 13: for the class $\alpha(1.4-1.5)$, upper left: relative dispersion (in percent) after successive filtering; upper right: selected phase functions; lower right: P_a mean value, lower left: relative dispersion for the selected P_a .

Figure 14: for the class $\alpha(1.4-1.5)$, retrieved phase function in the three CIMEL spectral bands (see symbols in the lower plot) from measurements in the principal plane (upper plot) and from the almucantar (lower plot).

Figure 15: $\alpha(670,440)$ versus $\alpha(870,670)$ for AEROPA at AAOT (cross) and 2Seas (square) and for WOPAER at AAOT (diamond) and 2Seas (triangle)

Figure 16: Same as figure 15 but for P_a at 90 deg. scattering

Figure 17: AEROPA single scattering albedo at AAOT: 870 nm versus 670 nm

Figure 18: WOPAER single scattering albedo at AAOT: 870 nm versus 670 nm

Figure 19: AAOT: Ratio of the WOPAER single scattering albedo 870 nm/670 nm versus the Angstroem coefficient.

Figure 20: same as figure 19 but versus the AOT at 670 nm.

1) Introduction

The knowledge of the aerosol optical properties is strong requirement for achieving the atmospheric correction over water in the frame of the analysis of the water colour. The aerosol optical properties were computed since several decades using standard aerosol models (R-1). These aerosol models were still used in the generation of the auxiliary data file (ADF) to feed the AC algorithms both for MERIS (R-2) and MODIS (R-3).

A worldwide network of photometers (AERONET) (R4) contributes since several decades to characterize the aerosols. The AERONET measurements are interpreted to give the aerosol inherent optical properties (IOP). These IOPs are used to generate LUTs first to predict the satellite signal (forward modeling). This approach was developed during the ISECA preparation (R5).

They are different approaches in the use of one AERONET data which combines at a given time multi spectral measurements of the extinction of the solar beam and of the sky radiance field:

(i) A direct transformation of the sky radiance into the aerosol phase function. ADRINORD followed this approach described in (R-6 & R-7) under the name of WOPAER. WOPAER was revisited and improved in the frame of ISECA and results are reported in (R-8).

(ii) The AERONET team proposes a micro physical description of the aerosols through the retrieval of standard size distributions of the aerosols associated to the aerosol refractive index (R-9). This micro physical description is available on the AERONET web server. We will denominate this approach AERONR.

(iii) This AERONET micro-physical description is used to compute the aerosol phase function at 3 wavelengths (440 nm, 670 nm and 870 nm). We will denominate this approach AEROPA.

The individual sets of IOPS can be used to generate one aerosol climatology. It was done:

(i) At a global scale for MERIS with WOPAER both over the land (R-10) and over the ocean (R-11).

(ii) For MODIS and SeaWiFS using AERONR over the ocean (R-12) at a global scale but accounting from the seasonal variability.

Because a direct link exists between AERONR and AEROPA, we can foresee that a aerosol climatology conducted with the two will be compatible.

The objective here is to propose a MERIS level 2 processing chain which relies on a regional climatology of the aerosols.

The regional climatology is based on the use of a regional AERONET network. This network has been described in (R-5) and the first task is to generate a climatology of the aerosol IOP based on what we reported in (R-8).

Section 2 will include the description of the AERONET measurements we used, the methodology we applied to realize the classes of IOP in the three CIMEL spectral bands starting from the aerosol IOP proposed by AERONET. This generation will be done for the 2Seas region using AEROPA but also in the AERONET station of shore of Venice (AAOT). The AAOT is a reference station for the MERIS validation. The introduction of another site allows investigating the spatial homogeneity of the aerosols. A deep analyze of the IOPs is reported in section 2.

Section 3 is devoted to WOPAER with an updated methodology to realize the IOP classes. Then, we analyse the WOPAER classes. Finally, a comparison between the two data sets (AEROPA and WOPAER) is reported.

2) The aerosol optical properties from AEROPA

2.1) The 2Seas and AAOT data base

In the A2 preparation phase, we identified and described the AERONET network in our area.

A data base of aerosol optical thickness (AOT) and phase functions is available in the AERONET web server. Table 1 gives for each AERONET station the number of individual measurement file with:

- (i) N1: total number of sequences of the aerosol phase functions
- (ii) N2: same as N1 but with the single scattering albedo

	N1	N2
Dunkerque	1096	173
Helgoland	520	44
Lannion	37	5
Oostende	1468	104
RameHead	10	0
De Hague	528	89
AAOT	5362	837
Total	9021	1252

Table 1: Number of sequences per station as described above for AEROPA

On a practical point of view, when we do not have a value of the single scattering albedo, it means that only the forward scattering radiance and the AOT are used to determine the aerosol model. When the single scattering albedo is provided, it means that the radiance in backscattering has been used.

2.2 –Ordering the AEROPA data base versus the Angstroem coefficient in the NIR

We now want to organize the data base versus the Angstroem coefficient in the NIR, defined as:

$$\alpha(\lambda, \lambda') = \frac{\log(\tau_a(\lambda)/\tau_a(\lambda'))}{\log(\lambda/\lambda')}, \quad (1)$$

The methodology will be evaluated with the AAOT data set which is the largest. We will start by the AERONET data base of Pa. We first report the single scattering albedo ϖ_0 , figure 1, which appears to be scattered versus α . Some points are out of scale and in figure 1, we filtered with:

$$0.85 < \varpi_0 < 1 \quad (2)$$

This filter will be applied in our processing when provided.

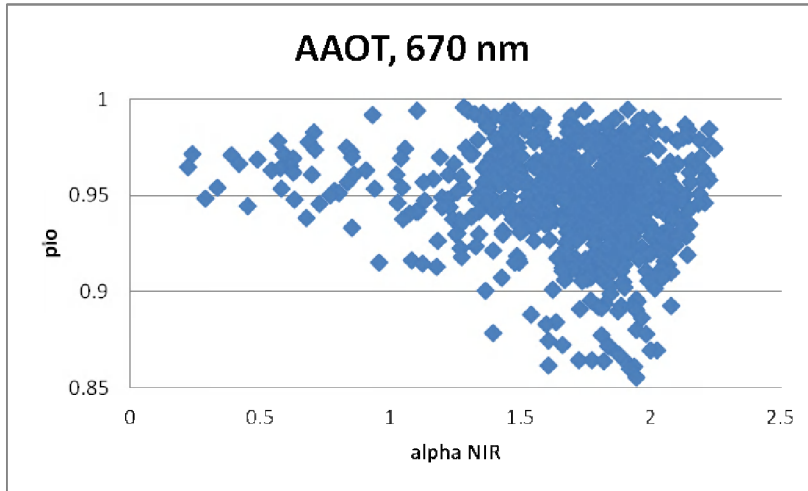


Figure 1: single scattering albedo versus the Angstrom coefficient for the Venice AERONET site.

The dispersion of the aerosol phase function is quite important at two wavelengths and two scattering angles as illustrated in figure 2. When we apply Eq. (2), figure 3, it does not change much at least for the range of α comprising a significant number of sequences. The decision is then to apply Eq. (2) to compute and to consider all the phase functions.

2.3 –Ordering the AEROPA data base versus the Gordon coefficient in the NIR

The Gordon coefficient, at a given scattering angle Θ , is defined by:

$$\varepsilon(\Theta, \lambda, \lambda') = \frac{\tau_a(\lambda)Pa(\Theta, \lambda) / (\tau_a(\lambda')Pa(\Theta, \lambda'))}{\log(\lambda/\lambda')}, \quad (3)$$

Or by:

$$\varepsilon'(\Theta, \lambda, \lambda') = \frac{\log(\tau_a(\lambda)Pa(\Theta, \lambda) / (\tau_a(\lambda')Pa(\Theta, \lambda'))}{\log(\lambda/\lambda')}, \quad (4)$$

A classification of Pa using ε' , figure 4, results in dispersion comparable to what we reported with α , figure 2.

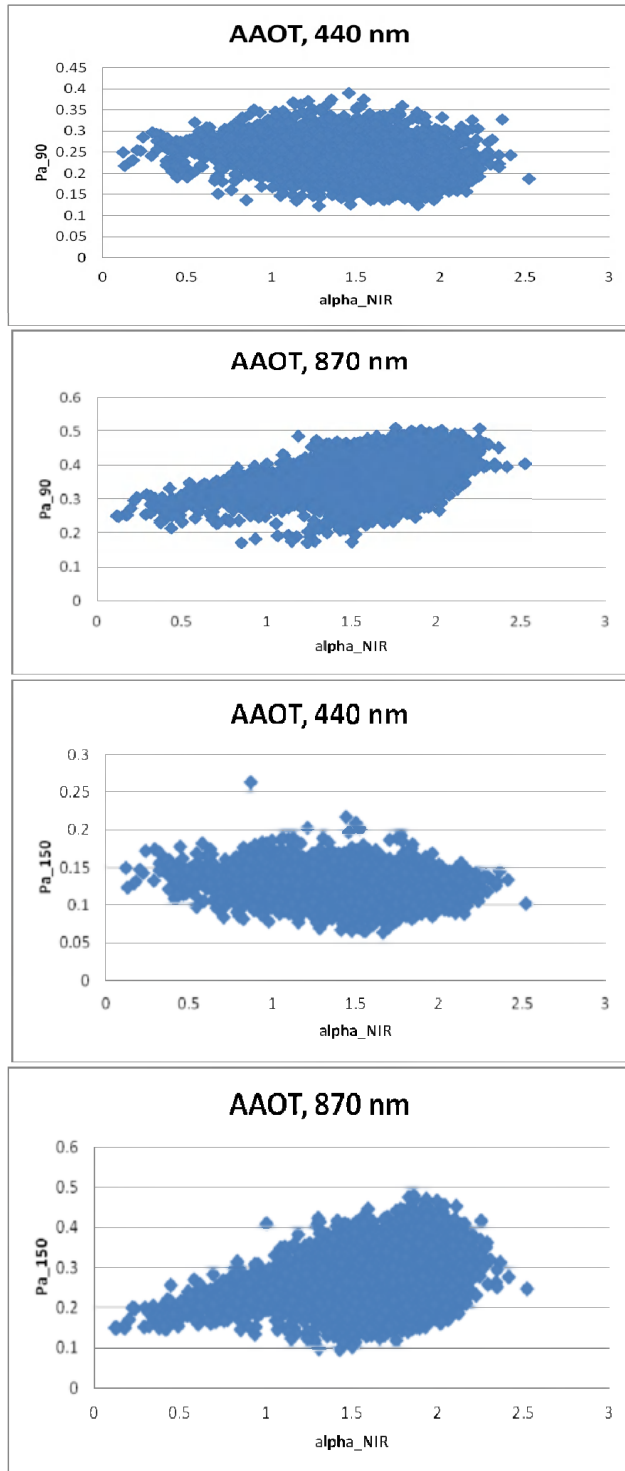


Figure 2: Aerosol phase function in two spectral bands for the 3562 sequences

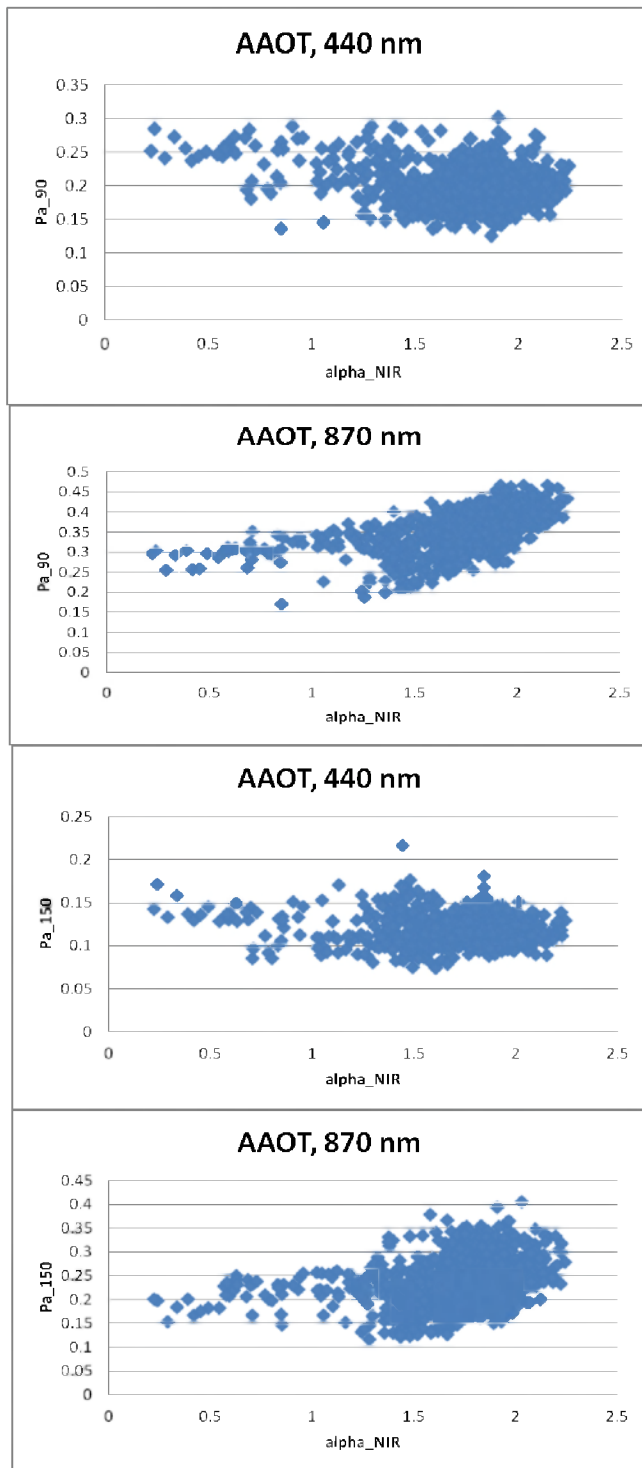


Figure 3: Aerosol phase function in two spectral bands for the 837 sequences

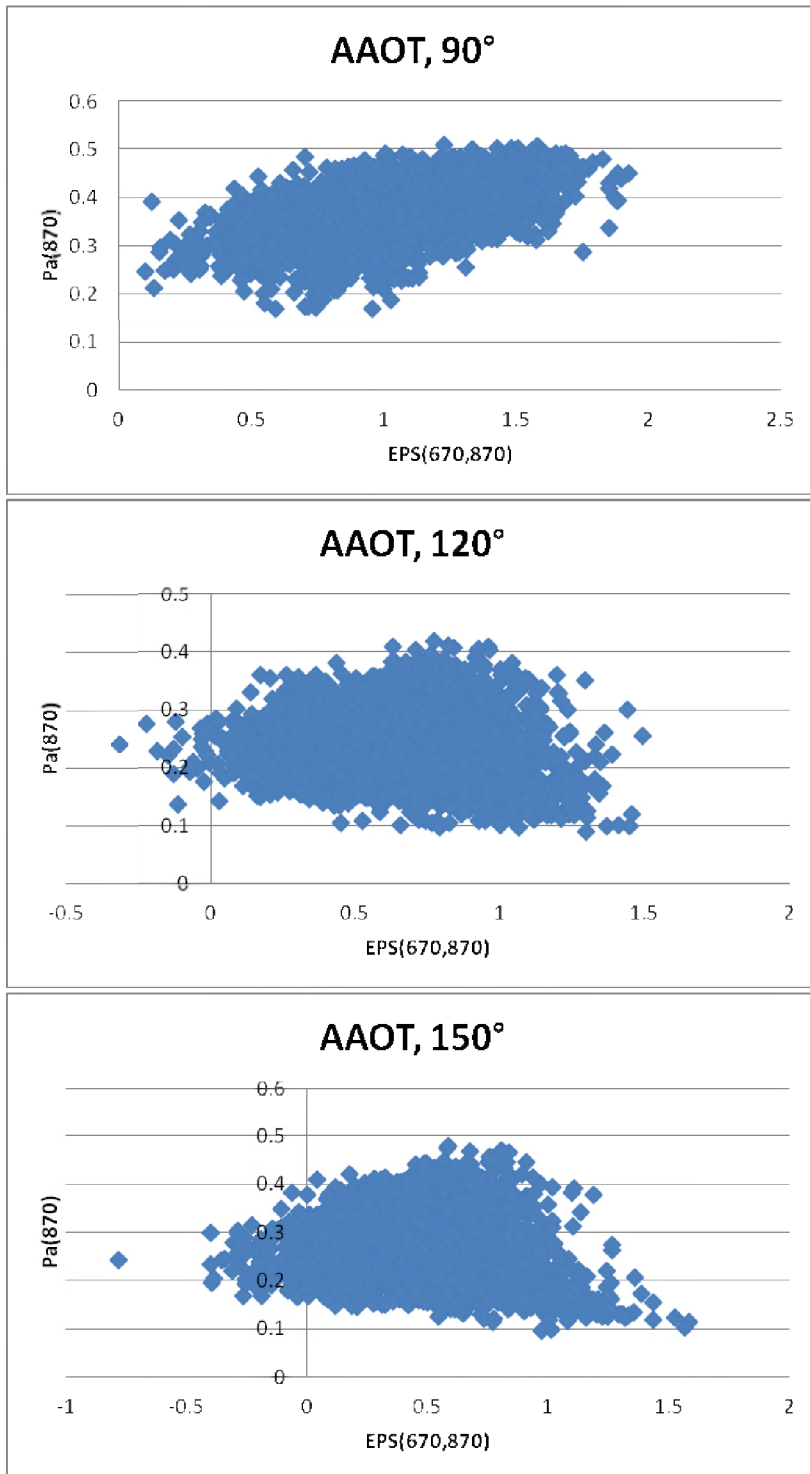


Figure 4: Aerosol phase function at 870 nm for three scattering angles: 90°; 120° and 150°.

The performance of the AC has not to be judged on the retrieval of the AOT but on the possibility to predict ϵ in the blue from ϵ in the NIR. More exactly, we extract the aerosol reflectance in the NIR and we want to know it in the blue. The quality control is knowing the spectral dependence of ϵ in the NIR how well do we know this spectral dependence in the blue? According to figure 5, starting from the knowledge of the spectral dependence of τ_{aPa} in the NIR, we have a large dispersion in the prediction of τ_{aPa} in the visible.

2.4 –The 16 classes of aerosol IOP

We defined 16 classes of IOPs to be in line with the number of standard aerosol models used for MERIS. The first model 1 is centered at $\alpha=0$; the increment is $d\alpha=0.15$ and the width of each class is 0.3. We also apply an iterative filter on τ_{aPa} :

- (i) At order 0, we compute the mean at the sigma for the 83 scattering angles and the three spectral bands.
- (ii) In an iterative loop, for the scattering angle domain (30° , 150°), we exclude sequences for which the relative dispersion is greater than 25 percent.

Table 2 illustrates the AAOT classification. The two first classes are almost empty which renders difficult to define the aerosol IOP for these two classes. On the other hand, the probability to see these two classes during MERIS matchups is low.

class	centre	N	alp_nir	alp_vis
1	0.00	2	0.12	0.22
2	0.15	9	0.20	0.33
3	0.30	42	0.36	0.56
4	0.45	83	0.46	0.70
5	0.60	122	0.60	0.88
6	0.75	171	0.74	1.08
7	0.90	228	0.89	1.25
8	1.05	319	1.04	1.35
9	1.20	525	1.19	1.45
10	1.35	846	1.33	1.51
11	1.50	1253	1.47	1.56
12	1.65	1758	1.61	1.62
13	1.80	1972	1.74	1.67
14	1.95	1401	1.86	1.74
15	2.10	554	1.98	1.83
16	2.25	119	2.10	1.93

Table 2: For each of the 16 class, we give the nominal centre in α , the number N of sequences per class, the Angstroem coefficients first between 670 nm and 870 nm; second between 440 nm and 670 nm.

The key parameter is $\epsilon(870,440)$ through the capability to extrapolate the aerosol path radiance from 870 nm to 440 nm, figure 6. 10 percent error on it directly results in 10 percent error on the retrieval of the aerosol reflectance in the blue following a single scattering approximation. The aerosol reflectance and the water reflectance in the visible are of the same order of magnitude. In other terms, in the AAOT it will be difficult to retrieve the water reflectance with accuracy better than 10 to 20 percent depending on the scattering angle. A vicarious adjustment may remove a bias but not dispersion.

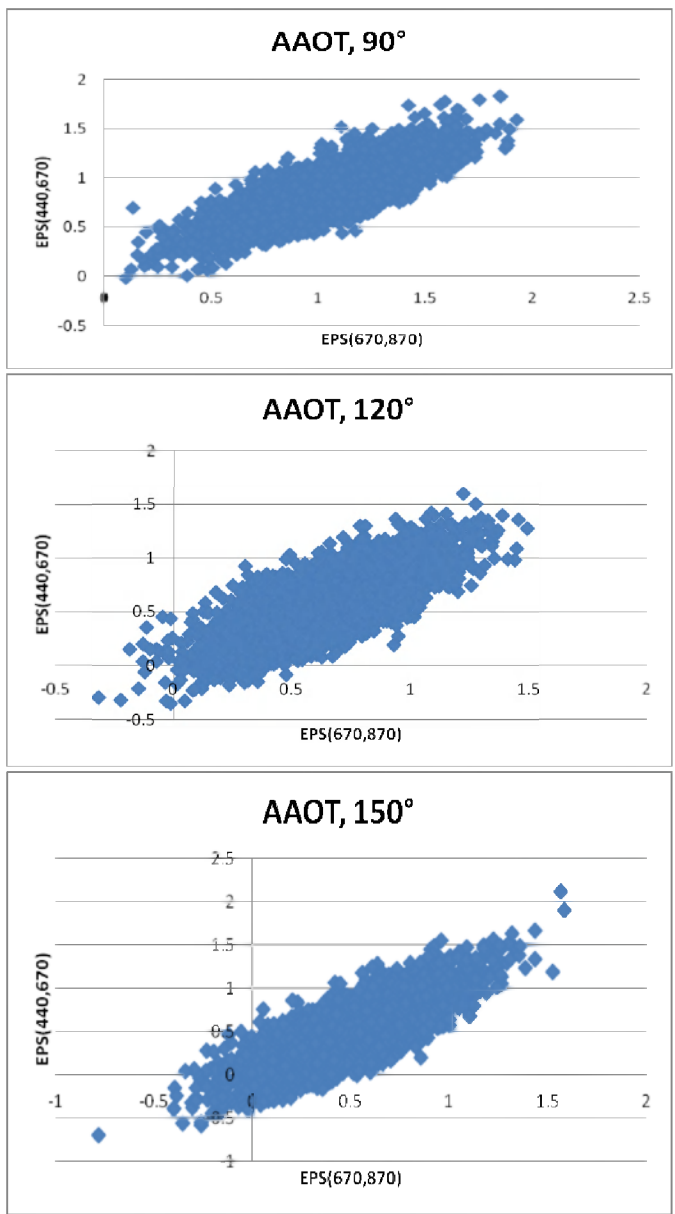


Figure 5: $\epsilon(440,670)$ versus $\epsilon(670,870)$ for three scattering angle

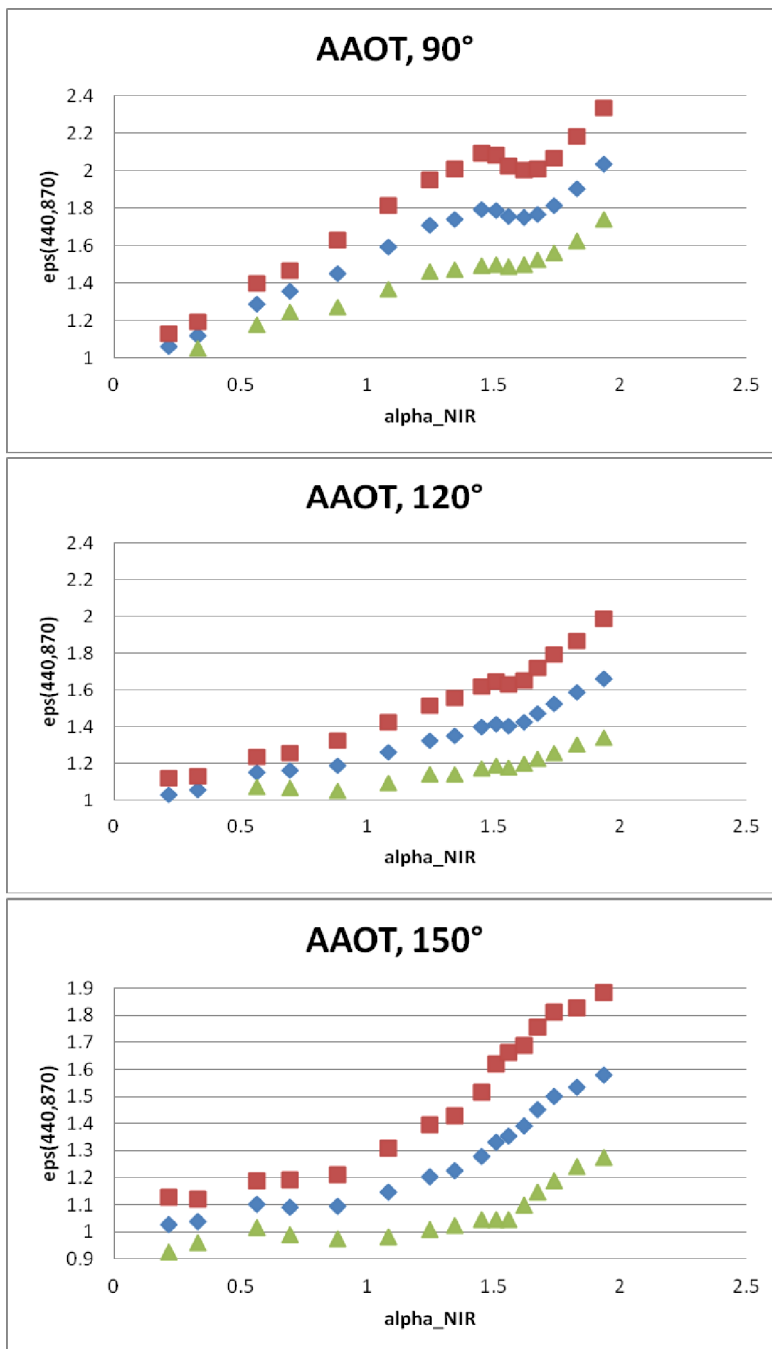


Figure 6: $\epsilon(440,870)$ for three scattering angles with the mean value (blue diamond), the maximum (red square) and minimum (green triangle) values at one sigma

2.5 –Detailed analysis of one class of AEROPA

The aerosol phase function

Within a class, the variation of Pa with α is not apparent, figure 7, but the dispersion remains substantial.

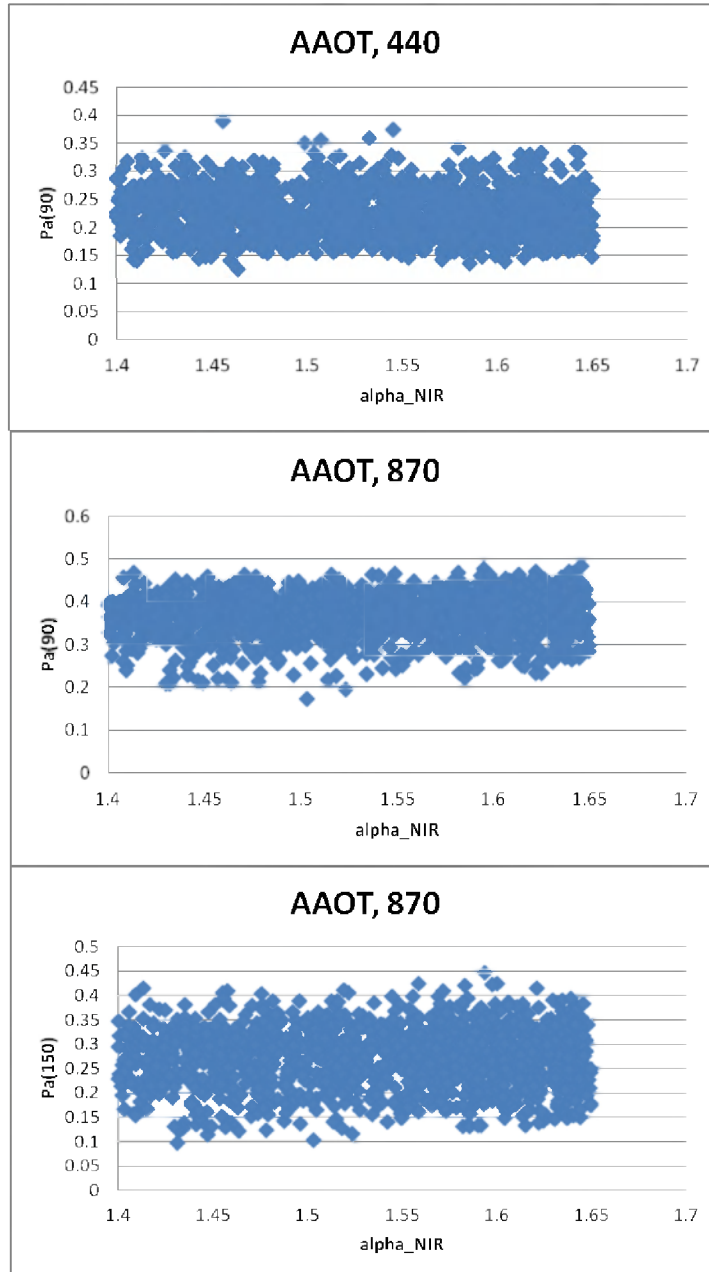


Figure 7: Dispersion of Pa in AAOT at two wavelengths for $\Theta=90^\circ$ and at 870 nm for $\Theta=150^\circ$.

Extrapolation of the aerosol reflectance from the NIR to the visible

Concerning the behavior of ϵ versus α , we do not see a trend, figure 8. It underlines the need or not to interpolate between two classes as it is done in MEGS.

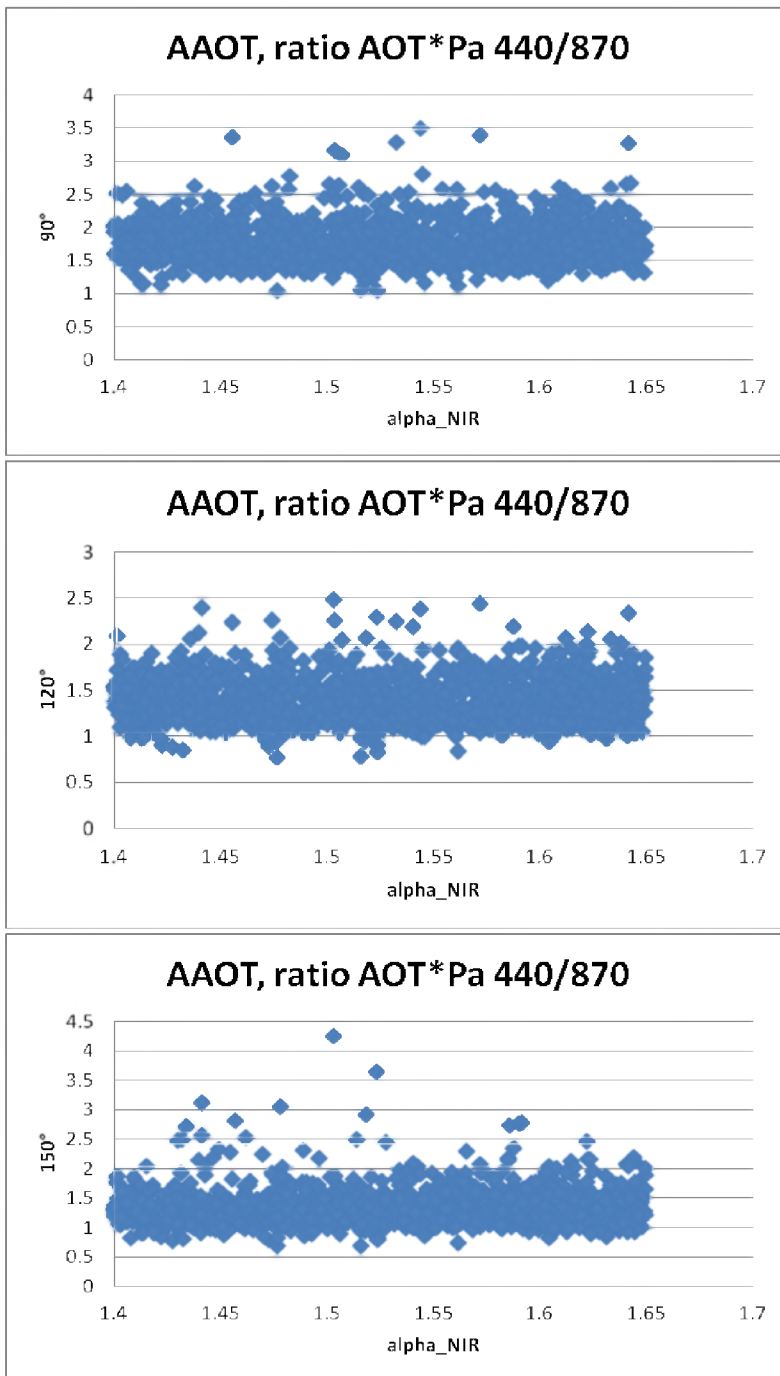


Figure 8: Dispersion of $\epsilon(440,870)$ in AAOT at three scattering angles.

Seasonal variability

On the AAOT, for the class#11, we did two subsets: winter includes November, December, January, February and March; summer includes May, June, July, August and September. The two sets are comparable:

- (i) In AOT, table 3
- (ii) In Pa, at least for the three selected scattering angles table 4.
- (iii) In ϵ , table 5.

This study may need to be consolidated for another AERONET stations for which the meteorology suggest the presence of seasonal wind regimes which may impact on the nature of the aerosols.

		AOT	440	670	870	alpha
Winter	mean		0.209	0.119	0.081	1.521
	501 sigma		0.213	0.139	0.095	0.085
Summer	mean		0.240	0.123	0.084	1.509
	722 sigma		0.199	0.124	0.085	0.086

Table 3: AOT (mean and sigma) in AAOT at 3 wavelengths and $\alpha(670,870)$

		440			670			870		
		90	120	149	90	120	149	90	120	149
Winter	mean	0.22	0.11	0.12	0.32	0.18	0.19	0.36	0.23	0.25
	sigma	0.04	0.02	0.02	0.06	0.04	0.04	0.05	0.05	0.06
	percent	18.42	17.19	16.64	17.30	23.25	22.68	14.90	22.60	23.41
Summer	mean	0.23	0.12	0.12	0.34	0.20	0.22	0.37	0.25	0.29
	sigma	0.04	0.02	0.02	0.05	0.04	0.04	0.05	0.05	0.06
	percent	16.48	16.08	14.39	14.37	19.52	20.10	12.18	18.48	20.19

Table 4: Pa (mean and sigma) in AAOT at 3 wavelengths and 3 scattering angles

		AOT_Pa(440,870)		
		90	120	149
Winter	mean	1.70	1.40	1.36
	sigma	0.28	0.25	0.35
	percent	16.37	17.96	25.98
Summer	mean	1.87	1.40	1.28
	sigma	0.28	0.23	0.28
	percent	15.24	16.31	21.86

Table 5: $\epsilon(440,870)$ (mean and sigma) in AAOT at 3 scattering angles

Regional variability

We now consider the two data sets: AAOT and 2seas. Figure 9 compares Pa at 440 nm. To indicate the dispersion of Pa, we plotted both Pa and Pa+ $\sigma\alpha$ in order to illustrate the dispersion. Of course by symmetry, we can imagine what Pa- $\sigma\alpha$ is. Clearly, the two sets differ but the dispersion is such that it is difficult to promote a regionalization of the aerosols for this case. The similitude between AAOT and the 2seas is even better on ϵ , figure 10.

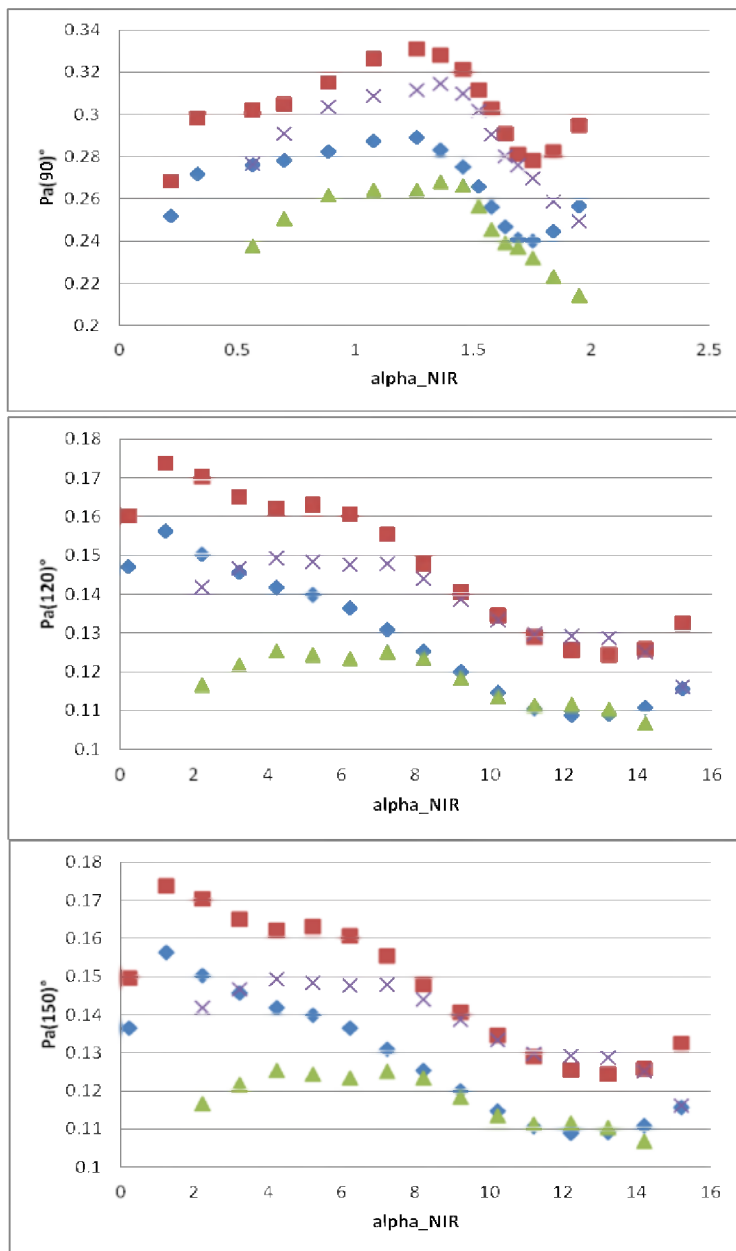


Figure 9: Comparison of Pa versus the Angstrom coefficient $\alpha(670,870)$ with the mean value for AAOT (blue diamond) and for the 2seas (green triangle) and the maximum values value for AAOT (red square) and for the 2seas (cross)

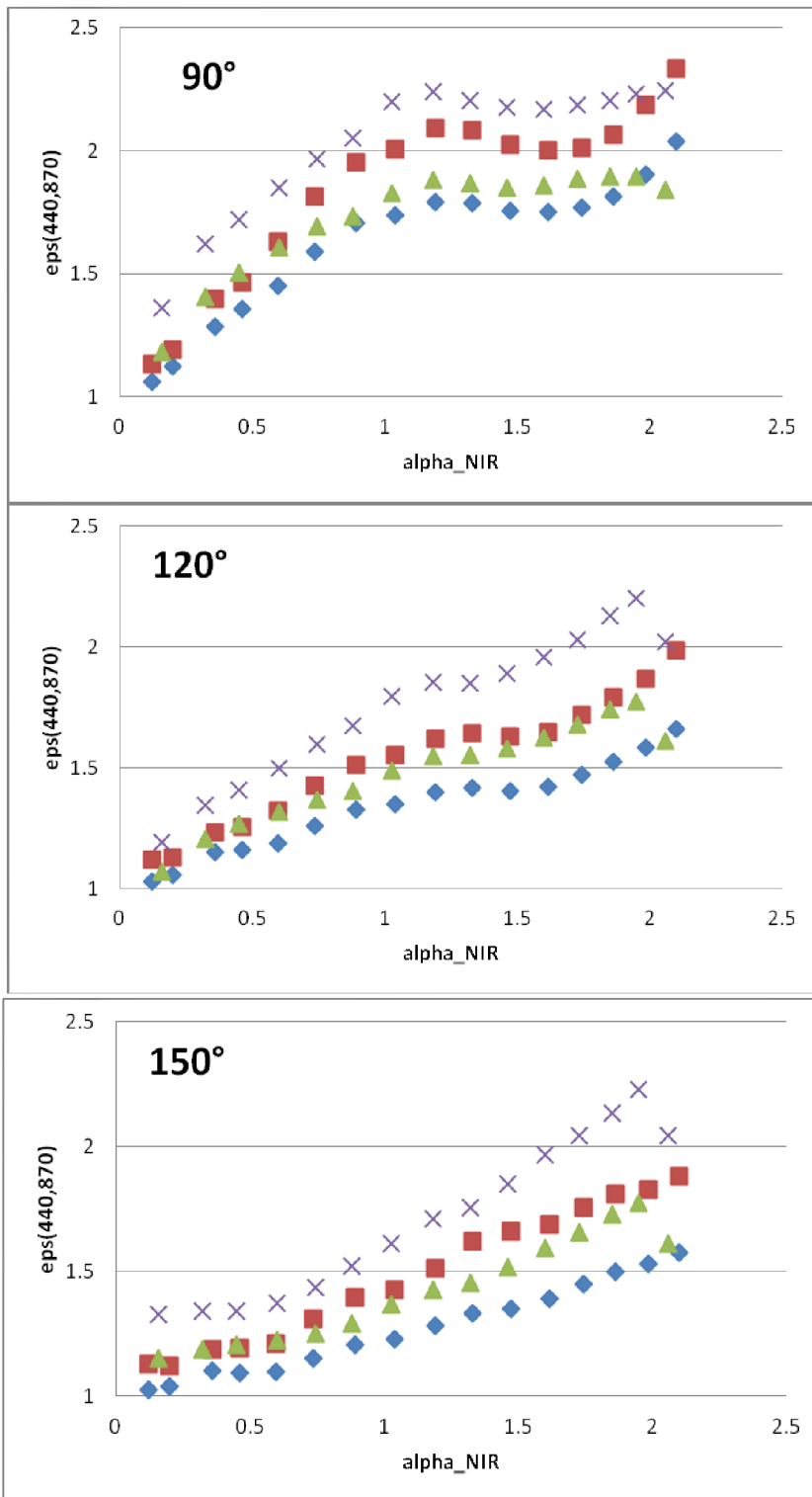


Figure 10: Same as figure 9 but on $\epsilon(440,870)$

2.6 –Conclusions and recommendations

Conclusion 1: It is not possible to describe with accuracy P_a , therefore you cannot have an accurate value of AOT_865. A validation through AOT needs a significant number of matchups to be valid in mean.

Recommendation 1: It is important to evaluate the impact of the poor knowledge of P_a on the water reflectance retrieval. An error bar can be generated through the use of maximum and minimum values of P_a and the spectral dependences of AOT.

Conclusion 2: When using ε instead of α , the dispersion is not really reduced.

Recommendation 2: Let's stay with the classification in α

Conclusion 3: There is no apparent seasonal variability of the aerosol IOPs. Because the water vapour content is low in winter compared to summer, it also means that the relative humidity may not be a key parameter.

Conclusion 4: There is no apparent regional variability of the aerosol IOPs.

3) The aerosol optical properties from WOPAER

3.1) Realisation of the 16 IOP classes from WOPAER

3.1.1) The heritage

Originally, WOPAER was applied at global scale on the AERONET network both over land and over ocean. (R-10 & 11). We defined 26 classes of aerosols using the Angstrom coefficient α between 670 nm and 870 nm. The width of each class is $d\alpha = 0.1$ and $0 < \alpha < 2.5$. These 26 classes correspond to the land processor (R-) but this class distribution was also used for the ocean processor.

The objective was first to provide the spectral variation of the AOT, with AOT_560 normalized to unit. We started by a normalization of the AOT at 550 nm. For each class of α , we made a 2nd order polynomial fit in a log-log scale on the AOTs at 440 nm, 550 nm, 670 nm and 870 nm.

Again for each class of α but for the phase function at 83 scattering angles Θ , we first averaged P_a and computed the r.m.s σ . For each Θ , a filter at 2σ is applied and we averaged P_a . This protocol is applied in the three CIMEL spectral bands for all the sequences collected in the principal plane and then in the two almucantars. For this massive data processing, we have thousands of sequences of P_a at a given spectral bands. It results that first we got a good angular continuity in the averaged P_a and second that P_a is normalized.

Comment [L1]: A confirmer!

For a regional application of this procedure as it is in the 2Seas region, we have a limited number of sequences. The results are reported in figure 11 at 870 nm for one class of aerosols. Clearly, the results at 440 nm still appear noisy and because of the aerosol scale height indetermination, the backscattering at 440 nm in the principal plane appears biased. At 870 nm, the plots appear smoother except that in the almucantar 1, the interception of a cirrus cloud on one sequence clearly impacts the final result.

Therefore, the performances of the initial filtering appeared suitable only for a significant number of sequences

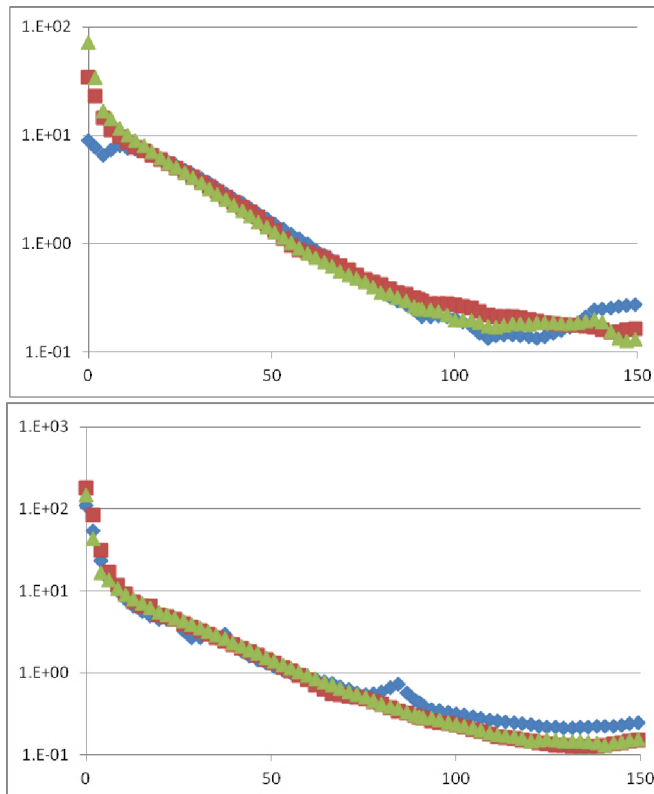


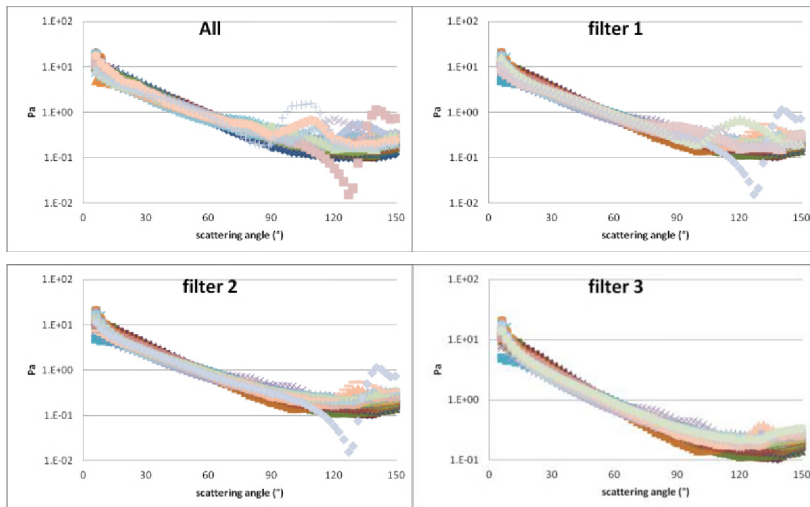
Figure 11: Retrieval of the aerosol phase function for the class $\alpha(1.4-1.5)$ at 440 nm (upper plot) and 870 nm in the principal plane (green triangles), the almucantar 1 (blue diamond) and 2 (red square)

3.1.2) The new approach

Always for the class $\alpha(1.4-1.5)$, we did plot in figure 12 all the retrieved P_a from measurements in the principal plane. As already noticed, we have lot of accidents probably related to the presence of finite clouds (cumulus, cirrus). Therefore, a filtering based on the dispersion of P_a in a large range of scattering angles is not suitable. Our strategy illustrated in figures 12 and 13 is the following:

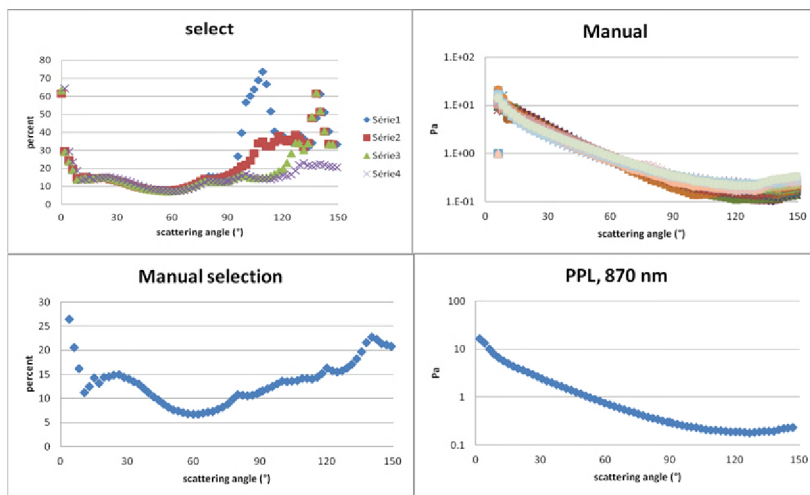
- (i) We take the mean and compute $\sigma(\Theta)$.
- (ii) We selected Θ for which the relative dispersion σ/mean is maxima. The first maximum (upper left of figure 11) occurred at $\Theta=115^\circ$. For this scattering angle, we filtered at σ and excluded all the sequences above to resume our filtering.

At the end, we filtered three times as illustrated in figure 12. We did that “manually” using excel and the selected sequences are reported in the upper right of figure 13. We stopped filtering when the maximum relative dispersion is less than 25 percent, the forward peak for $\Theta < 30^\circ$ being excluded. Here, we reached this criterion after three interactions to get (lower plots of figure 13) a smooth phase function with a reasonable dispersion.



26

Figure 12: Successive filtering of P_a for the class $\alpha(1.4-1.5)$



29

Figure 13: for the class $\alpha(1.4-1.5)$, upper left: relative dispersion (in percent) after successive filtering; upper right: selected phase functions; lower right: P_a mean value, lower left: relative dispersion for the selected P_a .

The new generation of the phase function is applied always for the class $\alpha(1.4-1.5)$, but for all the three wavelengths and the principal plane and the almucantar. Figure 14 illustrates the consistency of the P_a inversion between the principal plane and the almucantar. The only slight discrepancy occurred at 440 nm in backscattering as a result of the sensitivity in the blue of the principal plane measurement to the aerosol vertical distribution. We already noticed that to recommend to just use at 440 nm the almucantar results.

To conclude:

- (i) We redefine how to select the retrieved P_a to generate the mean of an aerosol class. , All P_a are first averaged and second we apply a filtering based on the relative difference between each sequence and the mean at 83 scattering angles. If for one angle, the relative difference is larger than 50 percent, we reject the sequence.
- (ii) We propose to average principal plane and almucantar at 870 nm and 670 nm.
- (iii) We propose to use in priority the almucantar at 440 nm.
- (iv) All the inverted P_a are distributed in the 16 classes as in §2.2.

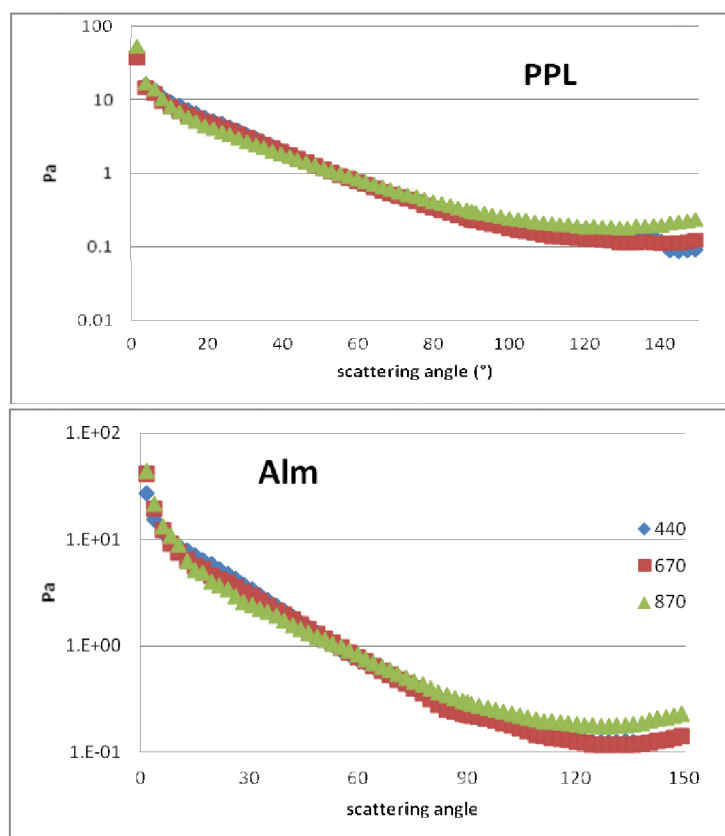


Figure 14: for the class $\alpha(1.4-1.5)$, retrieved phase function in the three CIMEL spectral bands (see symbols in the lower plot) from measurements in the principal plane (upper plot) and from the almucantar (lower plot).

3.2) The 2Seas and AAOT data base

Table 6 gives for each AERONET station the number of individual measurements processed as described above. It first reflects the climatology of the coastal aerosols (N0) with a clear peak around $\alpha=1.7$. Because of that, the first classes are empty. For the two sites, we have a total of 2109 compared to 9021 of Tab. 1. This difference is explained by the WOPAER selection of low solar elevations. N1 is rather small first because only the almucantar is inverted and second the inversion is problematic at large view angles. Nevertheless, if we have in mind that AEROPA only produces good inversion when ω_0 is retrieved,

$N2=1252$ of table 1 as to be compared to a total $N2=1716$ of table 6. In other word, the two sets are comparable.

	α	N0	N1	N2	N3	N0	N1	N2	N3
1	0.00	0	0	0	0	0	0	0	0
2	0.15	0	0	0	0	1	1	1	1
3	0.30	0	0	0	0	1	1	1	1
4	0.45	1	0	1	1	0	0	0	0
5	0.60	5	0	5	5	4	3	4	4
6	0.75	16	2	11	12	8	4	7	7
7	0.90	23	2	13	15	12	4	8	11
8	1.05	30	7	20	23	25	14	18	23
9	1.20	57	9	47	47	51	26	37	48
10	1.35	78	12	63	60	104	53	83	90
11	1.50	142	32	103	106	197	112	172	175
12	1.65	199	44	152	157	253	153	220	223
13	1.80	229	41	187	187	211	132	179	185
14	1.95	198	33	162	168	108	67	99	105
15	2.10	95	24	76	82	28	14	25	28
16	2.25	31	4	20	26	2	0	2	2
all		1104	210	860	889	1005	584	856	903

Table 6: Number of WOPAER sequences at each o the 16 classes (plus the total) for AAOT (left block) and the 2Seas region (right block) with N0: number of sequences before filtering; N1, N2, N3 number of sequences after filtering respectively at 412 nm, 670 nm and 870 nm.

3.3) Comparison of two methods

The first comparison brings on the AOT through α , Fig. 15. The 2 regions and the two sets are identical except when few individuals are present in a given class.

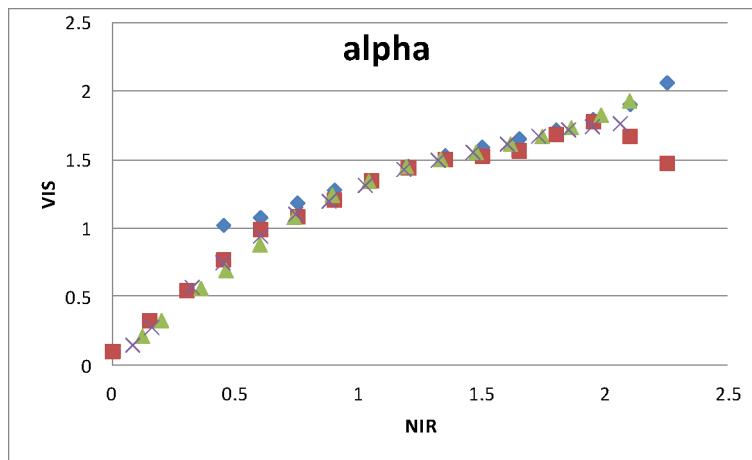


Figure 15: $\alpha(670,440)$ versus $\alpha(870,670)$ for AEROPA at AAOT(cross) and 2Seas (square) and for WOPAER at AAOT(diamond) and 2Seas (triangle)

Fig. 18 gives a comparison between AEROPA and WOPAER for the single scattering albedo at AAOT; but the same behavior exists in 2Seas. Let's forget the two first classes for AEROPA and α below 0.75 for WOPAER because the number of sequences we have is not representative. WOPAER indicates a substantial absorption in the red at 670 nm which does not exist in the blue and in the NIR. We carefully

checked the WOPAER outputs in this spectral band mainly to see if no trend exist with the AOT. It is not the case. This surprising result has to be understood.

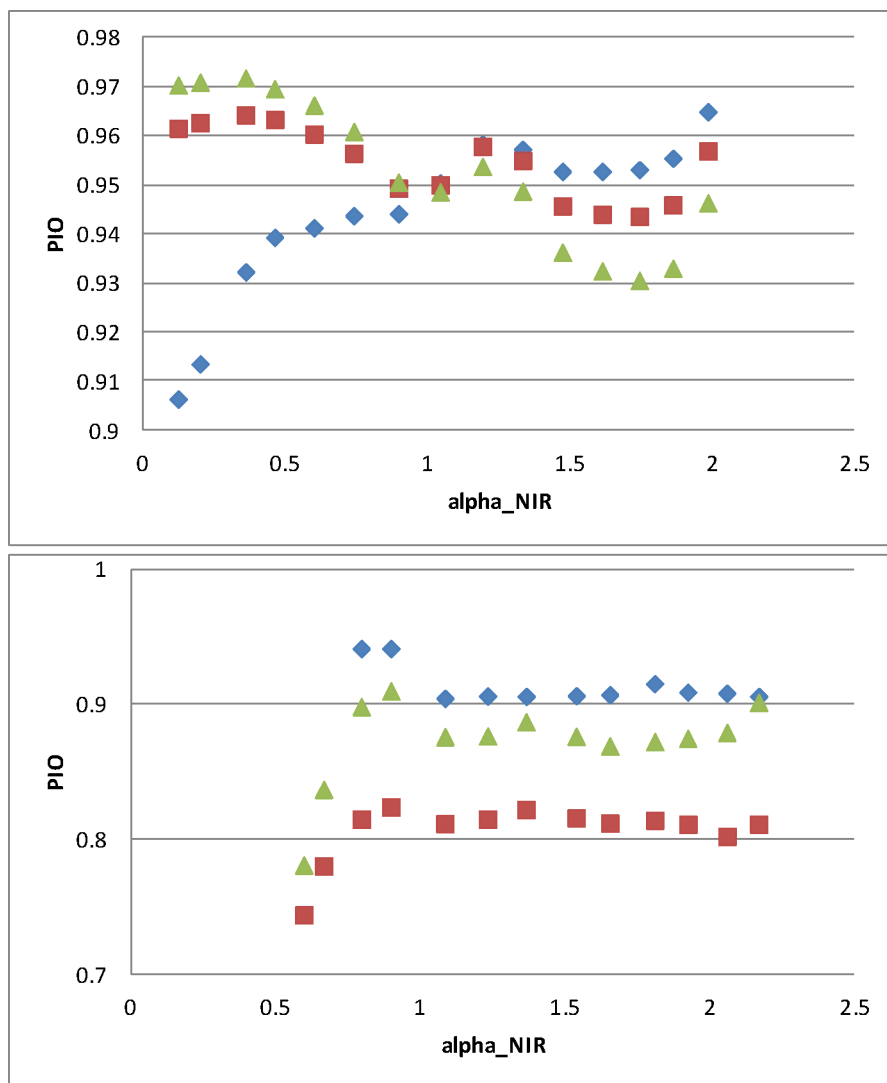


Figure 15: Single scattering albedo at AAOT from AEROPA (upper plot) and WOPAER (lower plot) at 3 wavelengths: 440 nm (diamond), 670 nm(square), 870 nm(triangle)

The similarity between AEROPA and WOPAER exists, figure 16, on the spectral behavior of P_a at a scattering angle of 90 deg. Nevertheless, substantial differences remain in absolute values.

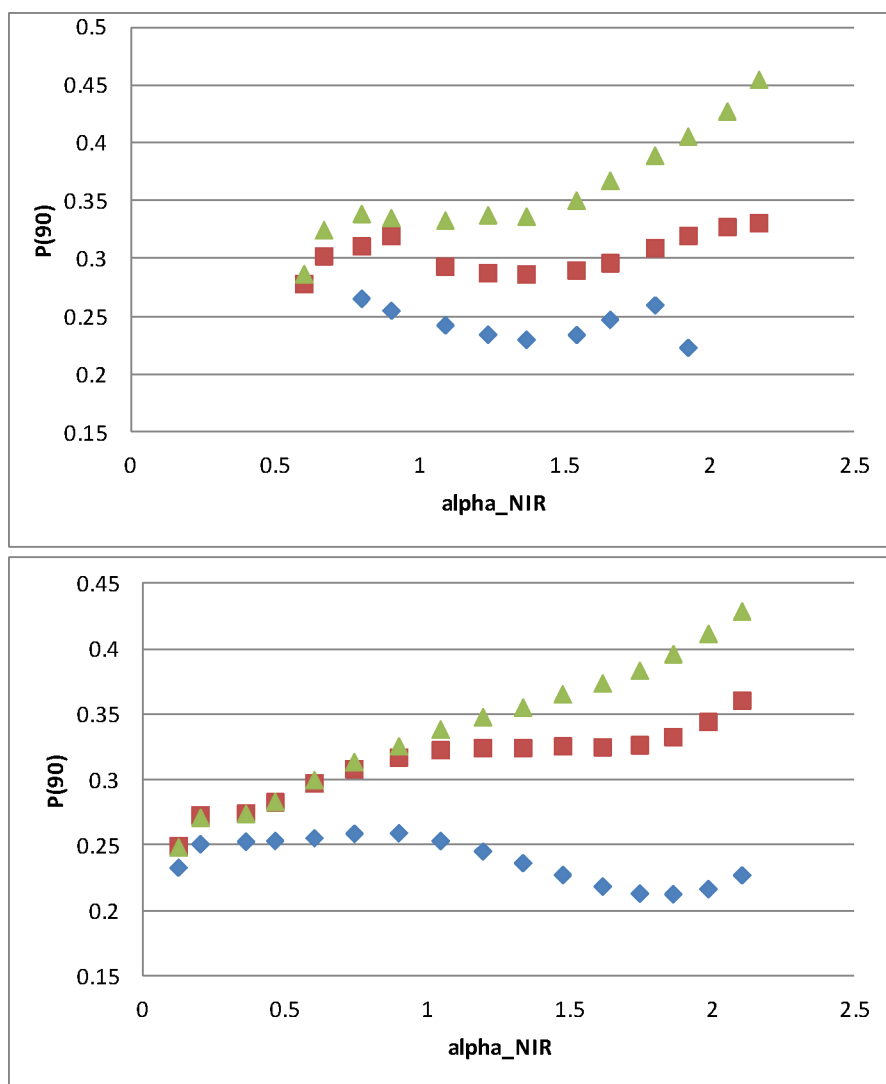


Figure 16: Same as figure 15 but for P_a at 90 deg. scattering

3.3) Single scattering albedo ω_0 at 670 nm

The results clearly differ at 670 nm between AEROPA and AERONET. AEROPA results from a theoretical computation with a small variability of the refractive index. Therefore what is proposed by AEROPA at AAOT, figure 17, corresponds to a negligible spectral variation of the single scattering albedo between the NIR and the red. It is not the case with WOPAER, figure 18, where ω_0 decreases by 8 percent between 870 nm and 670 nm. This decrease affects all the classes, figure 19. One possibility to explain an artificial decrease is to underestimate the atmospheric radiance, the WOPAER input. If so, after subtracting the Rayleigh contribution and used the normalization of P_a , it results in low values of ω_0 . It is the case if:

- (i) A wrong radiometric calibration results in underestimating the signal.

(ii) Or, the solar irradiance values used to convert the radiance into a normalized radiance is overestimated.

(iii) Or, the gaseous absorption correction is over estimated.

In the three cases, because we subtract the well know Rayleigh contribution (at 670 nm, the Rayleigh optical thickness is 0.04, we should see a trend with the AOT: for large AOTs, all the above bias have a decreasing impact.

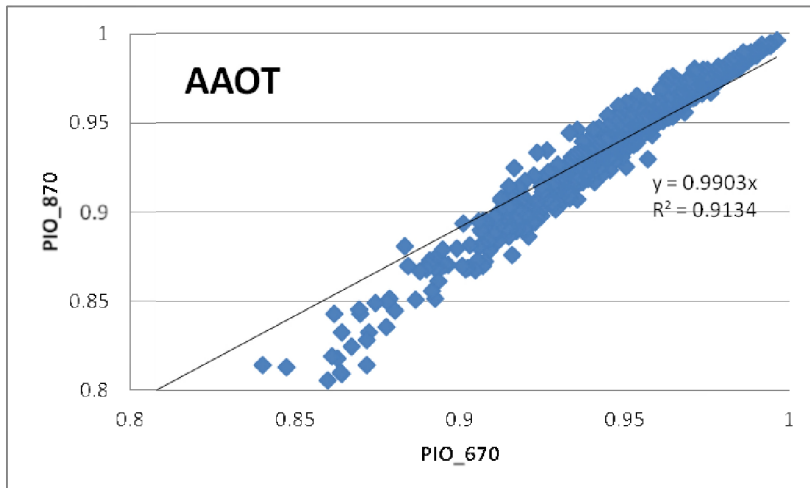


Figure 17: AEROPA single scattering albedo at AAOT: 870 nm versus 670 nm

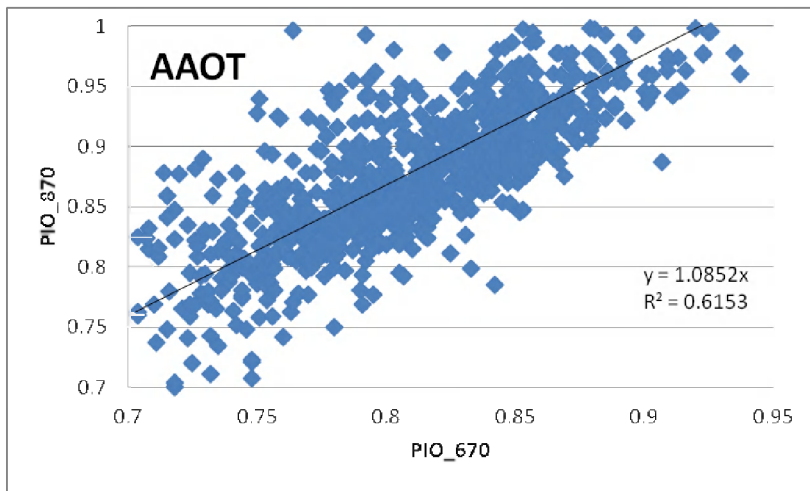


Figure 18: WOPAER single scattering albedo at AAOT: 870 nm versus 670 nm

Clearly, more investigations should be conducted and the first on them is to validate the WOPER processing chain on simulated radiance.

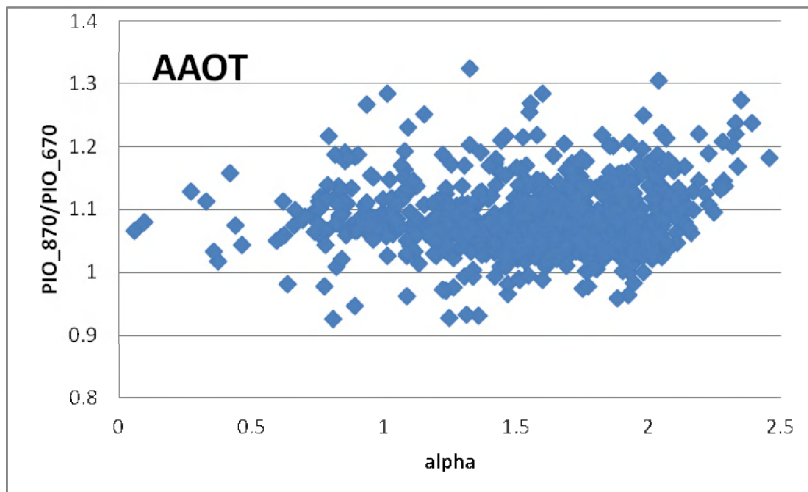


Figure 19: AAOT: Ratio of the WOPAER single scattering albedo 870 nm/670 nm versus the Angstroem coefficient.

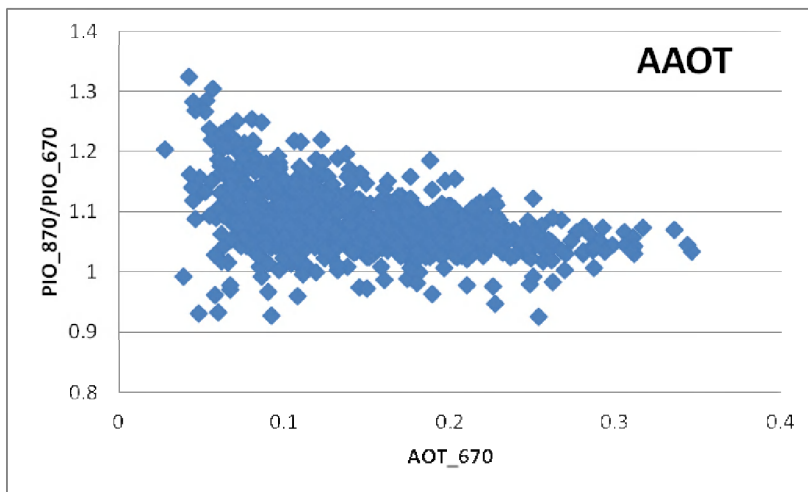


Figure 20: same as figure 19 but versus the AOT at 670 nm.

4 Conclusion

We first evaluated two different uses of the AERONET data. The advantages of AEROPA is to be stamped by NASA which means: important effort in developing the algorithms and document them, integration in an operational processing chain with quality control, public access and many feedback from the scientific community. The disadvantage is the need to rely on *a priori* assumption on the shape of the aerosols, their composition,... Also, the inversion is mostly based on the forward scattering and on the spectral dependence of the AOT. The first advantage of WOPAER is to convert the sky radiance into Pa with few physical assumptions (aerosol vertical distribution, contribution of the surface) and an expected limited impact on those assumptions because they are also used in the generation of the ADF. The second advantage of WOPAER is to use in priority the forward scattering, a geometry shared by the observations from space. The disadvantage of the two methods is the impossibility to access experimentally to the near backscattering (scattering angles larger than 150°).

The natural variability of the aerosol combined to the uncertainty of each method result in substantial errors in the retrieval of P_a or on the spectral dependence of the aerosol reflectance. The dispersion is more pronounced for small aerosols, which renders the atmospheric correction more challenging in coastal areas where they are compared to the open ocean. Within the dispersion, the two methods compared quite well as soon as a given class possesses a representative number of elements. The exception is the quite small SSA at 670 nm that WOPAER reports. Further checking of the result and a deeper analysis are required.

The dispersion of P_a suggests that a validation of the aerosol product restricted to the use of the AOT measurements may be not suitable. The measurement of P_a during matchups is required. This aspect is reported in a companion paper.

After the characterization of the aerosol IOPs, it is necessary to build an aerosol climatology in the context of the ADF generation. What we see in our analysis is first that the aerosol IOPs do not vary much from the south-western North Sea to the Adriatic Sea and second that seasonal effects are within the error bars.

A climatology driven by the micro-physic presents a risk in the continuity of the IOP versus the spectral dependence of the aerosol reflectance. It was the case for the MERIS SAM when the two bracketed models do not belong to the same family (maritime, urban,...). Than the reason why, we prefer to organize the data base with the IOP. All our plots versus $\alpha(670,870)$ indicated that this continuity exist.

We clearly have the inputs to produce error bars on the retrieval of the water reflectance values from space. We will see the results but we can already suspect that this task is difficult in coastal waters.

7) References

R-1 Shettle, E.P., and R.W. Fenn (1979), Models for the aerosols of the lower atmosphere and the effects of humidity variations on their optical properties, *Air Force Geophysical Laboratory, Technical Report AFGL-TR-79-0214*, Hanscom Air Force Base (Mass.).

R-2 Antoine, D., and A. Morel (2005), MERIS ATBD 2.7: Atmospheric Correction of the MERIS observations Over Ocean Case-1 waters, http://envisat.esa.int/instruments/meris/pdf/atbd_2_07.pdf

R-3 Gordon H. and Voss K. MODIS (1999) Normalized Water leaving Radiance Algorithm Theoretical Basis Document (http://modis.gsfc.nasa.gov/data/atbd/atbd_mod17.pdf)

R-4 Holben, B., T. Eck, I. Slutsker, D. Tanré, J.P. Buis, A. Setzer, E. Vermote, J. Reagan, Y. Kaufman, T. Nakajima, F. Lavenu, I. Jankowiak, and A. Smirnov, 1998. "AERONET – A federated instrument network and data archive for aerosol characterization", *Remote Sensing of Environment*, 66, pp. 1-16.

R-5 R. Santer and O. Aznay (2011) Atmospheric correction and related issues. ISECA report; Annex of the report on the preparation phase

R-6: Santer, R., and N. Martiny (2003), Sky radiance measurements for ocean color calibration-validation, *Applied Optics*, 42 (6), 896-907.

R-7 Santer, R., F. Zagolski, and O. Aznay, 2009. "Aerosol phase function derived from CIMEL measurements", *International Journal of Remote Sensing*, 31 (4), 969-992 ([doi:10.1080/01431160902912087](https://doi.org/10.1080/01431160902912087)).

R-8 O. Aznay, F. Zagolski, and Santer, R., 2012, Retrieval of the aerosol Inherent Optical Properties:

The new WOPAER processing chain. ISECA report

R-9 Dubovik, O., and M.D. King, 2000. "A flexible inversion algorithm for retrieval of aerosol optical properties from Sun and sky radiance measurements", *Journal of Geophysical Research*, **105**: 20673–20696.

R-10 O. Aznay, F. Zagolski, and Santer, R.,(2011) 'A new climatology for remote sensing over land based on the inherent optical properties', *International Journal of Remote Sensing*, 32: 10, 2851 — 2885.

R-11 F. Zagolski, Santer, R and O. Aznay,(2007). A new climatology for atmospheric correction based on the aerosol inherent optical properties. *Journal of Geophysical Research*, Vol. 112, No. D14, D14208

R_12 Ahmad, Z., B.A. Franz, C.R. McClain, E.J. Kwiatkowska, J. Werdell, E.P. Shettle, and B.N. Holben, 2010. "New aerosol models for the retrieval of aerosol optical thickness and normalized water-leaving radiances from the SeaWiFS and MODIS sensors over coastal regions and open oceans", *Applied Optics*, **49** (29): 5545-5556